

Effective Game-Theoretic Motion Planning via Nested Search

Avishav Engle, Andrey Zhitnikov, Oren Salzman,
Omer Ben-Porat, and Kiril Solovey

Technion–Israel Institute of Technology, Haifa, Israel
{avishav, andreyz}@campus.technion.ac.il, osalzman@cs.technion.ac.il,
{omerbp, kirilsol}@technion.ac.il

Abstract. To facilitate effective, safe deployment in the real world, individual robots must reason about interactions with other agents, which often occur without explicit communication. Recent work has identified game theory, particularly the concept of *Nash Equilibrium* (NE), as a key enabler for behavior-aware decision-making. Yet, existing work falls short of fully unleashing the power of game-theoretic reasoning. Specifically, popular optimization-based methods require simplified robot dynamics and tend to get trapped in local minima due to convexification. Other works that rely on payoff matrices suffer from poor scalability due to the explicit enumeration of all possible trajectories. To bridge this gap, we introduce *Game-Theoretic Nested Search* (GTNS), a novel, scalable, and provably-correct approach for computing NEs in general dynamical systems. GTNS efficiently searches the action space of all agents involved, while discarding trajectories that violate the NE constraint (no unilateral deviation) through an inner search over a lower-dimensional space. Our algorithm enables explicit selection among equilibria by utilizing a user-specified global objective, thereby capturing a rich set of realistic interactions. We demonstrate the approach on a variety of autonomous driving and racing scenarios where we achieve solutions in mere seconds on commodity hardware.

1 Introduction

Modern robotic applications—from autonomous driving to assistive robotics—require behavior-aware decision-making that accounts for interactions between the robot (the ego agent) and surrounding agents. These interactions often occur without explicit communication. Yet, to accomplish its mission effectively, the robot must reason about the behavior of other agents and the ways they respond to its actions. To address this challenge, this work seeks to advance the integration of game-theoretic reasoning into multi-robot decision-making by developing mechanisms that are both theoretically grounded and computationally efficient.

The majority of approaches for behavior-aware decision-making [29] consider a two-step process where the ego robot first predicts the actions of surrounding agents [16, 22, 30] and then computes a best-response trajectory that considers the agents as having fixed routes, or by reasoning over the probabilities of

taking various routes [33]. Such approaches overlook the fact that agents can update their actions based on the behavior of other agents, which can result in overly conservative solutions. In some cases, it can give rise to the “frozen robot” problem, wherein the robot deems all possible actions as overly unsafe and thus chooses to take no action.

More recent approaches aim to model interactions between agents through a game-theoretic perspective, thereby assuming that agents are rational and optimize a private objective function (e.g., travel time, safety, lead over opponent), while accounting for the fact that other agents are involved in the same process. For instance, some recent papers model interactions via a Stackelberg equilibrium and develop approaches based on dynamic programming to approximate the equilibrium [8]. However, Stackelberg games give an unfair advantage to one of the players [21], and hence lead to less realistic behavior. In the context of autonomous driving, such approaches can create overly aggressive maneuvers for one of the vehicles and be overly conservative for the rest.

More recent work is focused on modeling interactions via a Nash Equilibrium (NE) [26], which does not create an artificial advantage between agents. A NE implies that no agent is better off by unilaterally deviating from the current solution. Although the game theory community has extensively studied NE for many years [27, 34], most computationally-efficient results consider overly simplistic models that fail to capture the intricacies of real robotic systems, including continuous action and state spaces with non-convex constraints, as well as dependencies between the perception, planning, and control autonomy modules. For instance, some papers have attempted to approximate an NE using relaxations and utilizing differential dynamic programming [9], albeit with limited applicability to robotics due to the inability to capture collision-avoidance constraints.

More specialized approaches that incorporate hard collision constraints and robot dynamics have been recently introduced in the robotics community, where NE is approximated through optimization-based approaches [20, 21, 38, 41], albeit with limited theoretical justification. For example, [21] utilizes a first-order approximation and, as such, cannot guarantee finding a global NE except in some special convex settings, which rarely occur in robotics. Specifically, the presence of obstacles, nonlinear dynamics, and multiple agents gives rise to multiple homotopy classes of NE solutions, which cannot be captured in a convex approximation. The authors of [41] suggest an iterative approach, which relies on [38], but that falls short of the sufficient conditions for NE convergence, attaining only the necessary conditions. This is due to a lack of convexity in both cases, caused by “holes” (dynamic obstacles) in the feasible convex configuration space, induced by inter-robot collision constraints.

A different work [24] considers a mathematically principled approach for efficiently obtaining a NE from a set of precomputed robot paths, under special conditions, such as right-of-way, which benefits one of the agents. Unfortunately, in a general setting, the approach boils down to a brute-force computation of the NE via the full payoff matrix, which is exponential in the number of robots.

Moreover, the approach requires the explicit enumeration of all robot trajectories used, which can be costly if a rich set of strategies needs to be considered. A recent work [39] invokes the bi-matrix game reasoning of [24] in a receding horizon fashion to choose the immediate next action in a Stackleberg game, where the robots are confined to motions on a precomputed quasi-kinodynamic *graph* where edges represent Euler curves. Unfortunately, they provide no Equilibrium guarantees, and the use of Euler curves is highly problem- and model-specific.

Learning-based approaches have gained significant popularity in robotics in recent years and have been successfully applied in behavior-aware settings in the context of head-to-head racing in computer games [44], regulating mixed traffic flow [43], and autonomous driving [42], to name a few examples. However, as is typically the case with learning methods, they offer no explainability or generalizability and heavily rely on past experience for making correct decisions. Thus, their reliability remains unclear, especially in long tail events encompassing complex interactions between multiple agents [42].

To summarize, existing work in game-theoretic motion planning lacks sufficient theoretical grounding or practical scalability.

Contribution. We introduce an efficient and provably correct method Game-Theoretic Nested Search (GTNS) for computing a global NE for game-theoretic motion planning. Unlike aforementioned approaches in robotics, our method guarantees convergence to an NE without restricting the problem domain (e.g., convexity) and applies to general objective functions and dynamical constraints of individual robots. Furthermore, the approach enables the explicit tuning of the type of NE solution retrieved via a user-specified global objective function, ensuring that the returned NE minimizes this function among all available NEs. Examples of such global objectives include the sum of personal costs across all agents, or the cost of a specific competing agent.

At the core of our methodology is a nested-search approach consisting of an outer and inner search method. The outer search implicitly explores a tree of potential multi-robot trajectories, while the inner search is invoked to verify that a given solution satisfies the NE requirement by considering improving unilateral deviations of individual robots. This search-based approach allows for an implicit encoding of trajectory-based constraints and incremental reuse of information, which is otherwise difficult to realize efficiently within an optimization-based approach [3] or in methods that require explicit enumeration of all possible trajectories [24, 39].

For computational efficiency, our nested-search approach implicitly explores the joint state space of the multi-robot system via graphs that efficiently encode the trajectory space of individual robots while adhering to the robots' full dynamical constraints. We demonstrate the approach on a variety of realistic autonomous driving and racing scenarios (including intersections, lane merges, following distance, opposing-lane passes, and racetrack overtakes) where we achieve solutions in mere seconds on commodity hardware. From the theory side, our algorithmic framework leads to a rigorous but natural proof for the attainment of an NE.

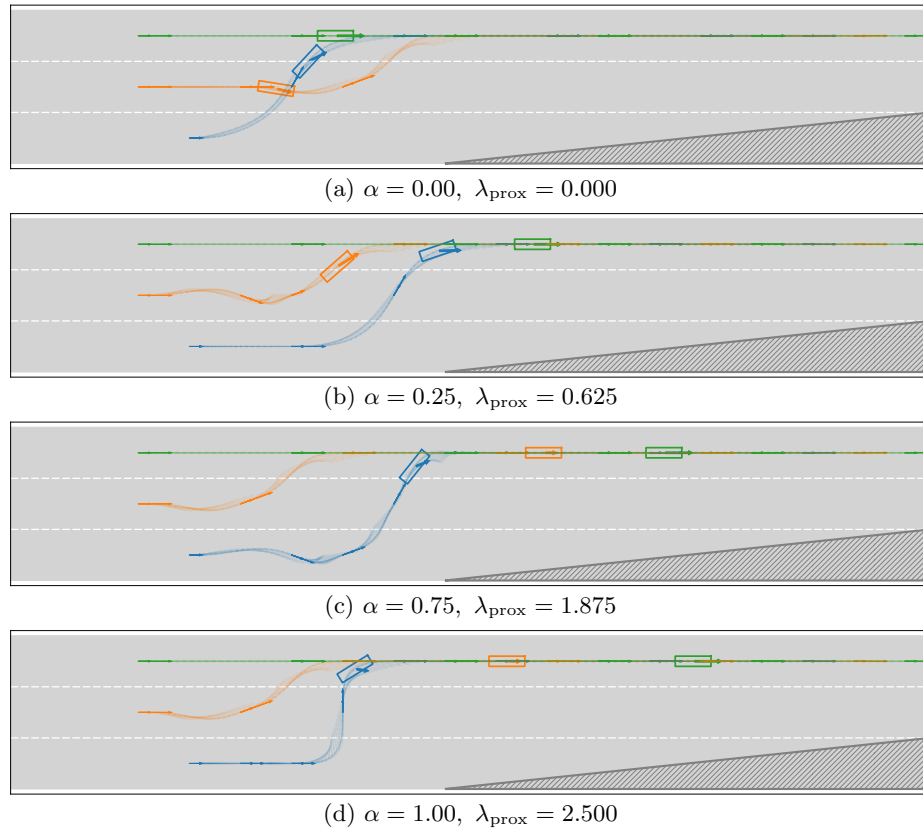


Fig. 1: Multi-lane merge: Robot 1 (blue) attempts to merge across Robot 2’s (orange) lane and into Robot 3’s (green) leftmost lane. Different NE regimes as Robot 1 priority decreases (larger α in $J = (1 - \alpha)J^1 + \alpha(J^2 + J^3)$) and proximity penalty weight λ_{prox} increases across panels (top→bottom). (a) aggressive zip-merge; (b) zip-merge; (c) yield-then-merge; (d) over-cautious merge.

Finally, we mention that our framework directly supports scalable generation of training data for generative AI and foundation models in autonomy [11, 16, 22, 30]. It enables rich simulation of multi-agent dynamics across domains (traffic, racing, aerial swarms, aircraft sequencing, warehouses) and can efficiently synthesize rare, safety-critical cases for training and evaluation.

Organization. This paper is organized as follows: Section 2 details the preliminaries of kinodynamic multi-robot motion planning and the game-theoretic concepts we employ, as well as declaring our problem statement and assumptions. In preparation of the search algorithm, Section 3 considers a graph-based formulation of the aforementioned problem. Section 4 describes in detail our algorithm GTNS, whose theoretical guarantees are then discussed in Section 5.

Finally, Section 6 details our experimental setup and results, highlighting the novel aspects of our algorithm and its running time.

2 Preliminaries

We begin by introducing the notation for kinodynamic multi-robot motion planning, then formalize the underlying game-theoretic planning problem.

Consider $m \geq 2$ robots indexed by $i \in [m] := \{1, \dots, m\}$. Each robot i has a state space $\mathcal{X}^i \subseteq \mathbb{R}^{d_i}$ and a control space $\mathcal{U}^i \subseteq \mathbb{R}^{D_i}$. Its motion is governed by the dynamics

$$\dot{x}^i(t) = f^i(x^i(t), u^i(t)), \quad x^i(t) \in \mathcal{X}^i, \quad u^i(t) \in \mathcal{U}^i. \quad (1)$$

Additionally, the robot must remain within the free space $\mathcal{X}_f^i \subseteq \mathcal{X}^i$ to avoid collisions with static obstacles (collisions with other robots discussed below).

Next, we consider robot trajectories resulting from integrating Eq. (1) for a given control law. For a given planning horizon $T > 0$, let \mathcal{U}_T^i be the set of admissible control functions $u^i : [0, T] \mapsto \mathcal{U}^i$ for robot i . Given an initial state $x_0^i \in \mathcal{X}^i$ and a control function $u^i \in \mathcal{U}_T^i$, the induced trajectory is the mapping $\pi_{x_0^i, u^i}^i : [0, T] \mapsto \mathcal{X}^i$, where $\pi_{x_0^i, u^i}^i(\cdot)$ is a solution to Equation (1) with $\pi_{x_0^i, u^i}^i(0) = x_0^i$. The set of feasible trajectories for robot i is

$$\Pi_T^i := \{ \pi_{x_0^i, u^i}^i \mid x_0^i \in \mathcal{X}^i, \quad u^i \in \mathcal{U}_T^i \}.$$

Next, we generalize the above definitions to encompass the full multi-robot system. The joint state space of the m robots is denoted by $\mathcal{X} := \times_{i=1}^m \mathcal{X}^i$, i.e., a point in \mathcal{X} describes the simultaneous state of all the robots in the system. Similarly, the joint control space is $\mathcal{U} := \times_{i=1}^m \mathcal{U}^i$ and the joint control space within specific time horizon T is $\mathcal{U}_T := \times_{i=1}^m \mathcal{U}_T^i$. Given initial joint state $x_0 = (x_0^1, \dots, x_0^m) \in \mathcal{X}$ and joint control $u = (u^1, \dots, u^m) \in \mathcal{U}_T$, the induced joint trajectory $\pi_{x_0, u} = (\pi_{x_0^1, u^1}^1, \dots, \pi_{x_0^m, u^m}^m)$ specifies the trajectories of each of the m robots, and can be interpreted as the mapping $\pi_{x_0, u} : [0, T] \mapsto \mathcal{X}$. The set of all joint trajectories is $\Pi_T := \{ \pi_{x_0, u} \mid x_0 \in \mathcal{X}, \quad u \in \mathcal{U}_T \}$.

Each robot i evaluates its performance via a cost functional

$$J^i : \Pi_T^i \times \Pi_T^{-i} \mapsto \mathbb{R}_{\geq 0},$$

where $\Pi_T^{-i} := \times_{j \neq i} \Pi_T^j$ is the set of trajectories of the remaining robots with indices $[m] \setminus \{i\}$. For trajectories $\pi^i \in \Pi_T^i$ and $\pi^{-i} \in \Pi_T^{-i}$,

$$J^i(\pi^i, \pi^{-i}) := \int_0^T c^i(\pi^i(t), \pi^{-i}(t)) dt, \quad (2)$$

with stage cost c^i depending on states and controls (e.g., control effort, distance to obstacles, proximity to others).

2.1 Problem Definition

In this work, we seek to compute joint trajectories that satisfy the following requirement.

Definition 1 (Nash Equilibrium). A joint trajectory $\pi = (\pi^1, \dots, \pi^m) \in \Pi_T$ is a (pure) Nash equilibrium (NE) if, for every robot $i \in [m]$ and for all alternative feasible trajectories $\tilde{\pi}^i \in \Pi_T^i$ (from the same start state), no robot can reduce its cost by deviating while the other robots fix their trajectories, i.e.,

$$J^i(\pi^i, \pi^{-i}) \leq J^i(\tilde{\pi}^i, \pi^{-i}). \quad (3)$$

Moreover, we are interested not only in finding any NE, but in selecting one that minimizes a user-defined global cost.

Problem 1 (Optimal NE Planning). Fix a planning horizon $T > 0$ and consider a global cost functional

$$J(\pi) := \int_0^T c(\pi^1(t), \dots, \pi^m(t)) dt, \quad \pi \in \Pi_T, \quad (4)$$

with stage cost c depending on joint states and controls.

We wish to find a joint trajectory $\pi^* \in \Pi_T$ (and its corresponding control laws) such that:

1. π^* is a Nash equilibrium (Def. 1);
2. π^* minimizes the global cost $J(\pi^*)$ among all NEs;
3. the final state of π^* is in the joint goal region, i.e., $\pi^*(T) \in \mathcal{X}_{\text{goal}} := \times_{i=1}^m \mathcal{X}_{\text{goal}}^i$;
4. $\pi(t) \in \mathcal{X}_f$ for all $t \in [0, T]$.

Discussion. A few comments are in order. We consider an *open-loop* setting: an NE solution is computed once for the horizon T and then executed, rather than replanned at every time step. This setting is common in robotics (see, e.g., [45]), motivated by the high computational demands of computing NEs, which currently preclude real-time feedback control. The resulting NE solutions promote stable execution, since local controllers cannot improve their cost by deviating from the prescribed trajectory.

Our formulation naturally extends to the ε -NE setting [40], in which no robot can improve its cost by more than a factor of $(1 + \varepsilon)$ through unilateral deviation, where Eq. (3) is replaced with the inequality

$$J^i(\pi^i, \pi^{-i}) \leq (1 + \varepsilon) J^i(\tilde{\pi}^i, \pi^{-i}). \quad (5)$$

We emphasize that we seek *global* NEs, where robots may choose any action in their control spaces. This contrasts with *local* NEs, which are implicitly considered in, e.g., [9, 21, 28, 38, 41], where the solution is restricted to a subset of the joint state space (e.g. due to linearization and convexification). Local NEs

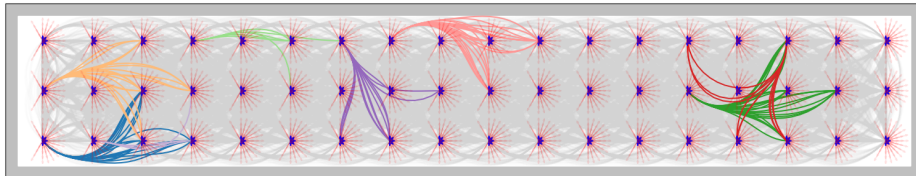


Fig. 2: Kinodynamic grid graph. Each discrete state $(x, y, \theta, v, \delta)$ is drawn with two arrows anchored at (x, y) : a blue heading arrow pointing in direction θ (fixed short length), and a red steering arrow pointing in direction $\theta + \delta$ with length $\propto v$. Graph edges are gray; a randomly selected subset is emphasized and color-coded by the source state.

may not correspond to any global NE, leading to unstable or otherwise poorly chosen execution. See illustration in Appendix A, Fig. 7.

Another key difference from prior work is our requirement that the chosen NE optimize a global objective. This promotes predictability and explainability, as (under mild conditions) a unique global optimum exists, ensuring all robots converge to the same NE even if using different algorithms. Without this constraint, agents may independently converge to distinct NEs that are not jointly valid, a source of instability noted in [21, 41], and tested in Section 6.

This framework can accommodate rich multi-agent preferences (e.g., effort $\int \|u\|^2$, comfort/jerk, rule compliance, barrier margins, connectivity/formation, visibility) via the user-defined objective, and in fact, even enables *targeting specific equilibria*: Let π be a target NE that yields per-agent costs $g^i := J^i(\pi^i)$, by choosing $J = \sum_i |J^i - g^i|$ as our global cost function, our algorithm finds the targeted NE π (upto tie-breaking between NEs with the exact same g^i 's).

A remaining challenge is incentivizing robots to follow the chosen solution. An NE optimizing J may favor certain robots, motivating others to defect. In cooperative domains (e.g., driving), J can encode social welfare or fairness and may even be set by an external arbitrator (e.g., to resolve right-of-way). In competitive settings, the more general solution concept of correlated equilibrium (CE) [2] could be applied: a mediator samples from a distribution and privately recommends actions. Every NE is a CE, but CEs enable coordination on outcomes that are more efficient or fair. In our setting, multiple solutions to Problem 1 could be combined into a CE by sampling between them with carefully chosen probabilities. This motivates extending our planner: instead of selecting a single NE, output a distribution over equilibria that all robots are incentivized to follow, since CEs guarantee no profitable unilateral deviations in expectation.

3 Graph-based setting

To tackle Problem 1, we draw inspiration from previous work on centralized (non-game-theoretic) multi-robot motion, wherein the curse of dimensionality, inherent in exploring the joint state space, is alleviated by first capturing the

state space of the individual robots via discrete graphs, and then planning their collective motion on an implicitly-defined tensor graph [36, 37]. In our setting, however, we utilize specialized constructions of those graphs to accommodate differential constraints (1) and, most importantly, game-theoretic aspects, which have not been considered in this context before. In preparation for our algorithm, which is described in the next section, we describe here the graph-based setting, as well as a graph-based counterpart of Problem 1.

3.1 Single-robot kinodynamic graphs

For each robot $i \in [m]$, we construct a *directed* graph $G^i := (V^i, E^i)$, that embodies its dynamically feasible motions. The vertex set $V^i \subseteq \mathcal{X}^i$ consists of sampled states, including the start state x_0^i and states in the goal region $\mathcal{X}_{\text{goal}}^i$. Each edge $e^i = (x^i, y^i) \in E^i$ corresponds to a dynamically feasible local trajectory $\pi_{e^i}^i$ from the state x^i to the state y^i obtained under some control law $u_{e^i}^i \in \mathcal{U}_{\Delta t}^i$, executed over a fixed duration $\Delta t > 0$ from the state $x^i \in \mathcal{X}^i$.

Every edge, therefore, represents a time-parameterized trajectory of duration Δt , making G^i a kinodynamic variant of the probabilistic roadmap (PRM) [17], as used in, e.g., [31, 32]. We note that each edge in the graph is a curve (kinodynamic-adhering trajectory) induced by the corresponding control function and not a straight line. We consider an explicit representation of each G^i ; more efficient semi-implicit constructions [15, 35] are left for future work.

3.2 Multi-robot tensor graph

From the individual graphs $\{G^i\}_{i \in [m]}$, we form the *tensor-product directed graph* $G = (V, E)$ with $V = \times_{i=1}^m V^i$, and $E = \times_{i=1}^m E^i$. A joint vertex $x = (x^1, \dots, x^m) \in V$ encodes a joint state of the m robots, while a joint edge $e = (e^1, \dots, e^m) \in E$ represents a local joint trajectory $\pi_e = (\pi_{e^1}^1, \dots, \pi_{e^m}^m)$ synchronized motion where each robot i follows the trajectory $\pi_{e^i}^i$ associated with the edge $e^i \in E^i$ during the same duration Δt . Since $|V|$ and $|E|$ grow exponentially in m , we never construct G explicitly; instead, we explore it implicitly by combining neighbors from the explicit graphs $\{G^i\}$, where an A*-search directs which portion of G to explore next (see below).

3.3 Graph-based problem formulation

Next, we adapt Problem 1 to the graph-based setting. Fix a number of steps $n \in \mathbb{N}_+$, such that $n\Delta t$ is equal to the planning horizon $T > 0$.

In the graph-based setting, a trajectory π_n^i of length n , corresponds to a path on the graph G^i , which consists of a sequence of n edges. That is, given the graph path e_1^i, \dots, e_n^i , the trajectory π_n^i is the concatenation of the trajectories $\pi_{e_1^i}^i, \dots, \pi_{e_n^i}^i$. We denote by Π_n^i the set of n -step trajectories of robot i . We similarly define the joint trajectory set $\Pi_n := \times_{i=1}^n \Pi_n^i$. Notice that each joint trajectory $\pi_n \in \Pi_n$ corresponds to a path on the graph G .

We emphasize that the although each trajectory $\pi_n \in \Pi_n$ is induced by a discrete graph, it represents a continuous and dynamically feasible motion for the robots in \mathcal{X} . As such, collision checking and evaluation of trajectory costs with respect to J, J^i are performed in the continuous domain.

Definition 2 (Graph Nash Equilibrium). *For a horizon of n steps, a joint discrete trajectory $\pi_n \in \Pi_n$ is a graph Nash equilibrium (gNE) if, for every robot $i \in [m]$ and every alternative trajectory $\tilde{\pi}_n^i \in \Pi_n^i$ (from the same start state), it holds that*

$$J^i(\pi_n, \pi_n^{-i}) \leq J^i(\tilde{\pi}_n^i, \pi_n^{-i}). \quad (6)$$

That is, no robot can reduce its cost by unilaterally deviating to another feasible n -step trajectory.

Problem 2 (Optimal gNE Planning). Fix $n > 0$. Given a global cost functional $J : \Pi_n \mapsto \mathbb{R}_{\geq 0}$ defined by (4), the objective is to find $\pi_n^* \in \Pi_n$ such that:

1. π_n^* is a graph Nash equilibrium (Def. 2);
2. π_n^* minimizes the global cost: $J(\pi_n^*)$ among all gNEs;
3. π_n^* reaches the joint goal region $\mathcal{X}_{\text{goal}}$ in n steps;
4. π_n^* is collision-free, i.e., all intermediate joint states and the continuous motions along edges respect \mathcal{X}_f .

Discussion. We discuss the interrelation between Problem 1 and Problem 2. Previous work has shown that for the geometric setting (i.e., without kinodynamic constraints), the graphs G^1, \dots, G^m can be constructed such that any feasible multi-robot trajectory in the continuous state space of the robot group can be approximated arbitrarily well in the graph G [4, 36]. The extension to the kinodynamic setting can be done via recent analysis techniques for asymptotically optimal sampling-based planning [18]. We leave this technical proof for future work. We note that the points highlighted in the discussion in Section 2, are equally applicable to the graph setting.

4 Algorithm for graph NE

We are ready to describe our algorithmic approach Game-Theoretic Nested Search (GTNS) to tackle Problem 2. The algorithm employs a nested approach, consisting of an outer search (Alg. 1) and an inner search (Alg. 2). Both levels of search are performed by A*-based search algorithms [12], albeit on different graphs and for different purposes.

4.1 Outer search

The GTNS algorithm (Alg. 1) explores the implicit tensor-product graph G induced by the per-robot graphs $\{G^i\}_{i \in [m]}$ produced by `generateRobotRoadmap`. These individual graphs can be precomputed once (offline) and reused across

scenarios for the same robot platform. By construction, motion along edges of G is dynamically feasible for all robots; along the way, we additionally enforce collision avoidance and the gNE condition.

The search is A*-style. It maintains a priority queue **OPEN** keyed by $J(\pi_x) + H(x)$ and a predecessor map P for path reconstruction. At each iteration, the algorithm: (i) extracts the minimum-key node x (line 4); (ii) recovers the current best path, denoted π_x , from the root using P (line 5); and (iii) enumerates neighbors X_{near} of x in G (line 6). Here X_{near} is the tensor product of the per-robot neighbor sets: a joint node $y = (y^1, \dots, y^m) \in V$ belongs to X_{near} iff for every i there is an edge $(x^i, y^i) \in E^i$.

For each potential neighbor $x_{\text{new}} \in X_{\text{near}}$, the algorithm (a) verifies that the local edge trajectory $\pi_{x \rightarrow x_{\text{new}}}$ is collision-free (line 8); (b) forms the candidate path $\pi_{x_{\text{new}}} := \text{concatenate}(\pi_x, \pi_{x \rightarrow x_{\text{new}}})$ (line 9); and (c) checks improvement w.r.t. any incumbent path to x_{new} (line 11), where the incumbent is recovered via P (line 10), which is later updated (line 13). It then calls the equilibrium predicate **ISNASHEQUILIBRIUM** on $\pi_{x_{\text{new}}}$ (line 12); only if the candidate satisfies the gNE condition is x_{new} inserted into **OPEN** with key $J(\pi_{x_{\text{new}}}) + H(x_{\text{new}})$. If a goal node is popped and validated, the corresponding trajectory is returned.

Algorithm 1: GTNS

```

1 OPEN  $\leftarrow \{x_0\}$ ;  $P(x) \leftarrow \emptyset, \forall x \in V$ 
2  $\{G^i\}_{i \in [m]} \leftarrow \{\text{generateRobotRoadmap}(f^i, J^i, x_0^i, \mathcal{X}_{\text{goal}}^i)\}_{i \in [m]}$ 
3 while not OPEN.empty() do
4    $x \leftarrow \text{OPEN.extractMin}()$ 
5    $\pi_x \leftarrow \text{trajFromRoot}(P, x)$ 
6    $X_{\text{near}} \leftarrow G.\text{neighbors}(x)$ 
7   for  $x_{\text{new}} \in X_{\text{near}}$  do
8     if collisionFreeEdge( $\pi_{x \rightarrow x_{\text{new}}}$ ) then
9        $\pi_{x_{\text{new}}} \leftarrow \text{concatenate}(\pi_x, \pi_{x \rightarrow x_{\text{new}}})$ 
10       $\pi_{x_{\text{new}}}^{\text{old}} \leftarrow \text{trajFromRoot}(P, x_{\text{new}})$ 
11      if notYetVisited( $x_{\text{new}}$ ) or  $J(\pi_{x_{\text{new}}}) < J(\pi_{x_{\text{new}}}^{\text{old}})$  then
12        if ISNASHEQUILIBRIUM( $\pi_{x_{\text{new}}}$ ) then
13           $P(x_{\text{new}}) \leftarrow x$  ▷ store parent
14          OPEN.insert( $x_{\text{new}}, J(\pi_{x_{\text{new}}}) + H(x_{\text{new}})$ )
15          if  $x_{\text{new}} \in \mathcal{X}_{\text{goal}}$  then
16            return  $\pi_{x_{\text{new}}}$ 
17 return  $\emptyset$ 

```

4.2 Inner search

ISNASHEQUILIBRIUM is a best-response oracle: it solves a single-robot motion planning problem on G^i to see whether any agent has a strictly cheaper unilateral

deviation of the same horizon that is dynamically feasible and collision-free w.r.t. others' fixed paths. For each candidate joint trajectory $\pi_{x_{\text{goal}}} = (\pi_{x_{\text{goal}}}^i, \pi_{x_{\text{goal}}}^{-i})$ encountered by GTNS, it calls (line 12) ISNASH EQUILIBRIUM (Alg. 2) which runs, for each $i \in [m]$, a standard A* search on G^i subject to three simple constraints:

- **Terminal-state constraint.** The search goal is the *specific* terminal configuration x_{goal}^i appearing at the end of $\pi_{x_{\text{goal}}}^i$ (no goal *region*); see the initialization above Alg. 2.
- **Horizon-length constraint.** Only paths of *exactly* n edges (garnered by the method numEdges) are considered competitive (the same length as $\pi_{x_{\text{goal}}}$). The code drops nodes once the partial path length d reaches n (the loop continues only while $d < n$).
- **Dynamic-obstacle constraint.** Edges for robot i are collision-checked against the *fixed, time-parameterized* trajectories of the other robots $\pi_{x_{\text{goal}}}^{-i}$; see the collisionFreeEdge method at line 13.

Operationally, for each i the routine initializes OPEN and a predecessor map P^i , then performs the usual A* node selection, neighbor expansion, concatenation, and incumbent comparison on the single-robot graph G^i (with key $J^i(\cdot) + H^i(\cdot)$), exactly mirroring the outer loop but *only* for agent i and under the constraints above. If it ever reaches x_{goal}^i in exactly n steps with a trajectory $\tilde{\pi}_{x_{\text{goal}}}^i$ yielding $J^i(\tilde{\pi}_{x_{\text{goal}}}^i) < J^i(\pi_{x_{\text{goal}}}^i)$, the routine immediately returns FALSE (the candidate joint trajectory does not meet the gNE conditions). If no robot can improve, the routine returns TRUE.

Remark. The pseudocode captures the high-level structure of the GTNS algorithm but omits several implementation optimizations for clarity. The most consequential (inspired by works such as [5]) is *lazy validation* of collision and equilibrium checks: every neighbour of x visited in line 7 is pushed to the OPEN list without immediate validation; only when a neighbour is popped from OPEN (i.e., it currently has the lowest cost) do we verify that it is in fact a valid node. This defers the most expensive computations and spends resources only on promising candidates. The implementation also caches edge-collision results (Boolean flags for whether an edge $e \in E$ is in collision) to allow a fast lookup before invoking an expensive check, it precomputes heuristics, and performs early feasibility checks for the query. Additional optimizations include careful memory management and the use of pointers to stable storage.

5 Theoretical guarantees

Below, we prove that Alg. 1 provides an optimal solution to Problem 2. In preparation, we obtain the following lemma that states that the NE property is monotone, i.e., every subtrajectory of a NE trajectory is also NE.

Algorithm 2: ISNASH-EQUILIBRIUM ($\pi_{x_{\text{goal}}}$)

```

1  $x_{\text{goal}}^i \leftarrow$  last vertex in  $\pi_{x_{\text{goal}}^i}^i$   $\triangleright \pi_{x_{\text{goal}}} = (\pi_{x_{\text{goal}}^i}^i, \pi_{x_{\text{goal}}^{-i}}^{-i})$ 
2  $n \leftarrow \text{numEdges}(\pi_{x_{\text{goal}}})$ 
3 for  $i \in [m]$  do
4   OPEN  $\leftarrow \{x_0^i\}$ ;  $P^i(x^i) \leftarrow \emptyset$ ,  $\forall x^i \in V^i$ 
5   while not OPEN.empty() do
6      $x^i \leftarrow \text{OPEN.extractMin}()$ 
7      $\tilde{\pi}_{x^i}^i \leftarrow \text{trajFromRoot}(P^i, x^i)$ 
8      $d \leftarrow \text{numEdges}(\tilde{\pi}_{x^i}^i)$ 
9     if  $d \geq n$  then
10      continue
11      $X_{\text{near}}^i \leftarrow G^i.\text{neighbors}(x^i)$ 
12     for  $x_{\text{new}}^i \in X_{\text{near}}^i$  do
13       if collisionFreeEdge( $\tilde{\pi}_{x^i \rightarrow x_{\text{new}}^i}^i, \pi_{x_{\text{goal}}^{-i}}^{-i}$ ) then
14          $\tilde{\pi}_{x_{\text{new}}^i}^i \leftarrow \text{concatenate}(\tilde{\pi}_{x^i}^i, \tilde{\pi}_{x^i \rightarrow x_{\text{new}}^i}^i)$ 
15          $\tilde{\pi}_{x_{\text{new}}^i}^{i, \text{old}} \leftarrow \text{trajFromRoot}(P^i, x_{\text{new}}^i)$ 
16         if not YetVisited( $x_{\text{new}}^i$ ) or  $J^i(\tilde{\pi}_{x_{\text{new}}^i}^i) < J^i(\tilde{\pi}_{x_{\text{new}}^i}^{i, \text{old}})$  then
17            $P^i(x_{\text{new}}^i) \leftarrow x^i$ 
18           OPEN.insert( $x_{\text{new}}^i, J^i(\tilde{\pi}_{x_{\text{new}}^i}^i) + H^i(x_{\text{new}}^i)$ )
19           if  $x_{\text{new}}^i = x_{\text{goal}}^i$  and  $d + 1 = n$  then
20             if  $J^i(\tilde{\pi}_{x_{\text{goal}}^i}^i) < J^i(\pi_{x_{\text{goal}}^i}^i)$  then
21               return FALSE
22 return TRUE

```

Throughout this section, given a trajectory π_n of n edges, the notation $\pi_{n'}$ for some $0 < n' < n$ denotes the subtrajectory of π_n consisting of the first n' edges. Namely, $\pi_{n'}$ has a duration of $n' \cdot \Delta t$ and $\pi_{n'}(\tau) = \pi_n(\tau)$ for any $0 \leq \tau \leq \Delta t \cdot n'$.

Lemma 1 (Monotonicity of Nash Equilibrium). *If trajectory π_n is a gNE (Def. 2) then any subtrajectory $\pi_{n'}$, where $0 \leq n' < n$, is a gNE too.*

Proof. Suppose that π_n is a gNE, namely for any robot $i \in [m]$, and any alternative trajectory $\tilde{\pi}_n^i \in \Pi_n^i$, with the same start and final \mathcal{X}^i state, i.e., $\pi_n^i(0) = \tilde{\pi}_n^i(0)$, and $\pi_n^i(n \cdot \Delta t) = \tilde{\pi}_n^i(n \cdot \Delta t)$, respectively, it holds that

$$J^i(\pi_n^i, \pi_n^{-i}) \leq J^i(\tilde{\pi}_n^i, \pi_n^{-i}). \quad (7)$$

Assume, by contradiction, that the subtrajectory $\pi_{n'}$, for some $0 < n' < n$, is not a gNE. I.e., for some robot $i \in [m]$, there exists $\tilde{\pi}_{n'}^i \in \Pi_{n'}^i$ satisfying the inequality

$$J^i(\pi_{n'}^i, \pi_{n'}^{-i}) > J^i(\tilde{\pi}_{n'}^i, \pi_{n'}^{-i}),$$

the collision constraints, $\pi_{n'}^i(0) = \tilde{\pi}_{n'}^i(0)$, and $\pi_{n'}^i(n' \cdot \Delta t) = \tilde{\pi}_{n'}^i(n' \cdot \Delta t)$.

We now consider the remaining portion of π_n from the $n' + 1$ edge, denoted by $\pi_{n'+1:n}$. I.e., $\pi_{n'+1:n}$ has a duration of $(n - n' - 1) \cdot \Delta t$ and $\pi_{n'+1:n}(\tau) = \pi_n(\tau + n' \cdot \Delta t)$. Next, denote by $\tilde{\pi}_n^i$ the trajectory resulting from concatenating $\tilde{\pi}_{n'}^i$ and $\pi_{n'+1:n}$. This new trajectory is valid since $\tilde{\pi}_{n'}^i$ ends where $\pi_{n'+1:n}$ begins, and both those subtrajectories are collision free. Moreover, by exploiting the additivity of the cost function J^i , we upper bound the J^i cost resulting from $\tilde{\pi}_n^i$:

$$\begin{aligned} J^i(\tilde{\pi}_n^i, \pi_n^{-i}) &= J^i(\tilde{\pi}_{n'}^i, \pi_{n'}^{-i}) + J^i(\pi_{n'+1:n}^i, \pi_{n'+1:n}^{-i}) \\ &< J^i(\pi_{n'}^i, \pi_{n'}^{-i}) + J^i(\pi_{n'+1:n}^i, \pi_{n'+1:n}^{-i}) = J^i(\pi_n^i, \pi_n^{-i}). \end{aligned}$$

This contradicts Equation (7). Thus, the gNE property must be monotone. \square

Combining the above lemma, with the optimality guarantee of A* graph search, which is the backbone of both Alg. 1 and 2, we establish the correctness of GTNS.

Theorem 1. *GTNS finds the optimal solution to Problem 2.*

Proof. Recall that running the A* algorithm returns an optimal solution when running on a search problem P using an admissible heuristic [12]. Recall that a search problem is a tuple $P = \langle S, \text{Succ}, s_{\text{begin}}, S_{\text{goal}} \rangle$, where S is a set of (abstract) states, $\text{Succ} : S \rightarrow 2^S$ is a successor function mapping each state to a set of neighboring states, $s_{\text{begin}} \in S$ is the initial state and $S_{\text{goal}} \subset S$ a set of goal states.

We start by formalizing our problem as a search problem and then continue to show that Alg. 1, which can be seen as an adaptation of A*, inherits its optimality. Specifically, consider the search problem defined over the set of states $S = V$ (i.e., each abstract state represents a joint vertex, which in itself represents a joint robot state). The successor function is defined such that for vertices $v, v' \in V$, we have that $v' \in \text{Succ}(v)$ if and only if $(v, v') \in G$. Finally, the start and goal states are x_0 and states satisfying Problem 2.

Alg. 1 can be seen as an adaptation of A* where nodes are only added to the OPEN list if they satisfy equilibrium conditions (line 12) and using an admissible heuristic H . Pruning search nodes in this search problem does not hinder optimality of the search due to the Nash monotonicity property (Lemma 1). That is, search nodes that are pruned cannot contribute to a longer trajectory that is a NE. Thus, optimality follows from the optimality of A*. As noted, Alg. 2 is too an adaptation of A*, and thus when used with an admissible heuristic, returns an optimal, collision-free path of upto length n . \square

6 Experiments and Results

We provide an experimental evaluation of our game-theoretic approach in driving and racing scenarios. We begin this section with implementation details and

experiment setup, along with a discussion of the kinodynamic graph construction. We then proceed to a qualitative evaluation showcasing the behavior of the approach. Then we evaluate the computational and scalability aspects of our approach. We conclude with experiments examining the effect of the mismatch between the NE solutions chosen by individual robots, and the effects of limited short-horizon NE solutions, that can be computed using previous bimatrices approaches [24, 39], as compared to our own approach (which is more scalable in terms of horizon length).

6.1 Implementation details and problem setting

The single-robot graphs G_i are built offline in Python using CasADi `Opti` [1] for BVP solving (see more information below). GTNS is implemented in C++ on a LEMON [7] graph library backbone, and is executed online. All simulations were run on a 64-bit laptop with an Intel Core i9-14900HX CPU (2.20 GHz) and 32 GB RAM, running Windows 11. The experiments did not rely on GPU acceleration.

For the robot model, we consider the second-order bicycle model [19], which models nonholonomic steering while remaining lightweight enough for real-time planning. The robot has the states, controls, and dynamics, of the form

$$\mathbf{x} = \begin{bmatrix} x \\ y \\ \theta \\ v \\ \delta \end{bmatrix}, \quad \mathbf{u} = \begin{bmatrix} a \\ \omega \end{bmatrix}, \quad \dot{\mathbf{x}} = \begin{bmatrix} v \cos \theta \\ v \sin \theta \\ \frac{v}{L} \tan \delta \\ a \\ \omega \end{bmatrix},$$

respectively. Here x , y and θ are the 2-D positions and heading of the car, v , and δ are its speed and steering angle, and a and ω control their rate of change. L is the distance between front and rear axles (wheelbase). We use a scale-model car of length $l = 0.70$ m, width $w = 0.20$ m, and wheelbase $L = 0.50$ m. Collision checking uses a circular footprint of radius $r_{\text{coll}} = \sqrt{l^2 + w^2}/3$. See Appendix A, Fig. 8 for visualization.

Kinodynamic graphs. For the single-robot graphs G^i , we consider two constructions. The *grid graph* (Fig. 2) samples a spatial lattice in (x, y) (with $\Delta x = \Delta y = 1$ m) and enumerates headings, speeds, and steering angles on discrete sets (θ, v, δ) (with $\Delta v = 1$ m/s and $\Delta\theta, \Delta\delta$ specified per map). From each node we attempt directed connections to *nearby* nodes within a k -hop neighborhood of the lattice. The *track graph* (Appendix A, Fig. 9) samples along a track centerline with lateral offsets: at each longitudinal sample we define a wayline (normal to the centerline), set the heading from the centerline tangent, and discretize (v, δ) as above. From each wayline ℓ we attempt connections from all nodes on ℓ to all nodes on any wayline ℓ' with $|\ell' - \ell| \leq k$. In both graph types, nodes represent states $(x, y, \theta, v, \delta)$ within bounds $\theta \in (-\pi, \pi]$, $v \in [0, 10]$ m/s, $\delta \in [-\pi/2, \pi/2]$. Unless otherwise stated, robots share identical dynamics and graph G^i .

Our choice of graph type is guided by two complementary paradigms. The *grid graph* is task-agnostic: it covers arbitrary workspaces with obstacles and is suitable for general multi-robot scenes. By contrast, the *track graph* leverages road/track topology—known centerline and lane structure—to align headings with geometry, reduce unnecessary branching, and permit longer, better-conditioned local connections between nearby waylines. In practice, the track graph tends to be smaller and sparser, enabling faster search for driving/racing scenarios, whereas the grid graph provides uniform coverage when no privileged centerline exists.

Graph size is determined by the sampling resolutions $(\Delta x, \Delta y, \Delta \theta, \Delta v, \Delta \delta)$ and the connection parameter k . We choose these to meet a computational budget while preserving sufficient fidelity for the maneuvers of interest. Concretely, we set spatial and angular resolutions and k to reach a desired ballpark of nodes/edges, then prune infeasible nodes/edges via kinodynamic feasibility and obstacle inflation. The resulting sizes per graph for a selection of graphs are reported in Table 1.

Edge generation is performed in the following manner. For each candidate source→target pair of nodes, we solve a fixed-duration two-point boundary-value problem (BVP) over $\Delta t = 1$ s. We transcribe the dynamics via direct collocation using forward-Euler integration, i.e., we discretize the horizon into $N = 22$ uniform steps of size $\Delta \tau = \Delta t/22$ and enforce the dynamics at the grid points while treating controls as zero-order hold on each step:

$$z_{j+1} = z_j + \Delta \tau f(z_j, u_j), \quad j = 0, \dots, N - 1.$$

In practice, this means we choose the piecewise-constant control sequence u_0, \dots, u_{21} (and the corresponding knot-point states) that drives the model from the source to the target over 1 s while respecting bounds, with boundary conditions $z_0 = \text{source}$, $z_N = \text{target}$ and hard input limits $|a| \leq 5 \text{ m/s}^2$, $|\omega| \leq 2 \text{ rad/s}$. If the BVP is feasible, we add the corresponding directed edge and store its continuous trajectory. Edges are discarded if their continuous trajectory intersects obstacles inflated by r_{coll} . Unless otherwise specified, each edge has unit cost.

Search heuristics For each robot i we precompute all-pairs shortest-path distances on G^i (APSP) and use $H(x) = \sum_i H^i(x^i)$ where H^i is the single-robot shortest distance from x^i to $\mathcal{X}_{\text{goal}}^i$. Because single-robot distances satisfy the triangle inequality and joint costs add across robots, H is consistent (and hence admissible) on the tensor-product graph G . Moreover, during inner A* searches for robot i on G^i with dynamic obstacles induced by a fixed plan π^{-i} , H^i remains a valid lower bound on i 's cost-to-go: the added constraints only restrict feasible motion and cannot reduce the optimal single-robot cost.

6.2 Qualitative analysis

We present a set of scenarios mimicking interactions between multiple agents in autonomous driving and racing and discuss the results obtained using our algorithm.

Across tasks we vary two interpretable knobs that shape the resulting NE.

1. *Priority in the **global** objective.* The global objective aggregates the individual costs $J(\pi_n) = \sum_{i=1}^m \alpha_i J^i(\pi_n^i, \pi_n^{-i})$ to encode priorities via the weights α_i .
2. *Proximity (safety) inside each **individual** cost.* Each J^i includes a state-based penalty that discourages small separations from other robots:

$$c_{\text{prox}}^i(\mathbf{x}^i, \mathbf{x}^{-i}) = \frac{\lambda_{\text{prox}}}{\max(\min_{j \in -i} \|P(\mathbf{x}^i) - P(\mathbf{x}^j)\|_2, \varepsilon)},$$

where $\lambda_{\text{prox}} \geq 0$, $P: \mathcal{X} \rightarrow \mathbb{R}^2$ returns the planar position (x, y) of a state and $\varepsilon=10^{-3}$ prevents singularities (yielding a bounded, well-behaved, Lipschitz stage cost). Larger λ_{prox} promotes greater standoff.

In our experiments, each J^i is the sum over n edges of π_n^i of unit edge cost plus the proximity term for each of the $n + 1$ nodes along the way:

$$J^i(\pi_n^i, \pi_n^{-i}) = n + \sum_{\mathbf{x}^i \in \pi_n^i} (c_{\text{prox}}^i(\mathbf{x}^i, \mathbf{x}^{-i})),$$

so $\{\alpha_i\}$ weights *between* agents at the global level, while λ_{prox} shapes *within*-agent costs that the search optimizes on each edge.

Next, we discuss the scenarios and the solution obtained by GTNS.

Four-way intersection. We consider a single-lane four-way intersection with perpendicular approaches by two robots, objective $J = \alpha J^1 + (1-\alpha)J^2$, $\alpha \in [0, 1]$, $\lambda_{\text{prox}} = 0$. Fig. 3 shows that increasing α selects the NE in which Robot 1 proceeds and Robot 2 yields; decreasing α selects the opposite NE. This result illustrates the ability of our NE planner to select a safe NE in an explainable manner (via tuning of the objective function J), without requiring clipping of the dynamics or costs, or initial guesses (as commonly considered in previous work).

Racetrack overtake. We consider a S-curve racetrack segment to showcase priority-driven overtaking decisions between two robots. This setting probes how a scalar priority α biases raceline choice and pass timing within realistic behavioural dynamics trajectories captured by the NE framework. Here, we set $J = \alpha J^1 + (1-\alpha)J^2$, $\alpha \in [0, 1]$, $\lambda_{\text{prox}} = 0$.

Fig. 4 shows that the tilt of robot priority determines which robot targets the inside line at the final turn, and ultimately wins the race. It is important to note however, that even at high α , Robot 1 is blocked at the early corner—illustrating that even in the best NE for Robot 1, overtaking early is not feasible due to kinodynamic/safety constraints. This too is a significant result as we can (using our tuned NE, and finding the best NE for a given robot) robustly express the lower bound on the cost of a given robot’s solution (within the space of all NEs). That is to say, that using our algorithm, we can discern, for example,

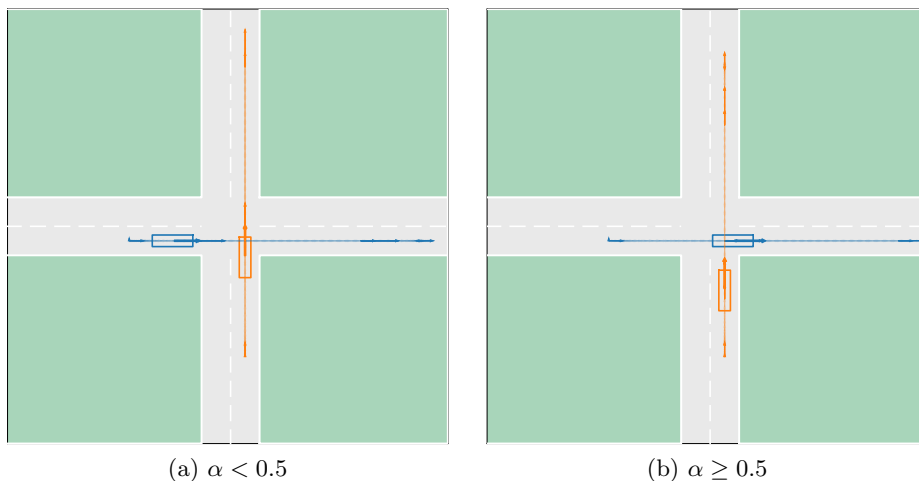


Fig. 3: 4-Way Intersection. Robot 1 (blue) crosses left→right, Robot 2 (orange) down→up. Robots cross in priority order, with the other waiting for the intersection to clear before proceeding.

when a loss is imminent, no matter what, and act accordingly (prioritize low damage and fuel burn, for example, conserving resources for subsequent tasks).

Following distance. Here, we consider a more complex racetrack segment and evaluate how proximity weight affects behaviour in semi-collaborative setting, such as two cars on the same F1 team, with social welfare cost $J = \sum_i J^i$ and $\lambda_{\text{prox}} \in [0, 1]$.

The effect of the proximity penalty is clear in Fig. 5, with small λ_{prox} yielding close drafting, and larger values increasing the time-gap as the trailing car deliberately backs off (visible at the first corner). This result shows the strength of our algorithm for solving global NE, with (almost) generic costs.

Multi-lane highway merge. We consider a three-lane highway merge with three robots to explore homotopy classes of merge options as α and λ_{prox} trade priority against risk. We set $J = (1 - \alpha)J^1 + \alpha(J^2 + J^3)$, $\alpha \in [0, 1]$, and $\lambda_{\text{prox}} \in [0, 2.5]$.

We can see in Fig. 1 complex behavioural changes. As priority for Robot 1 decreases and λ_{prox} increases, the NE transitions through: (i) *aggressive zip-merge* (tight gaps); (ii) *calm zip-merge* interleaving; (iii) *yield-then-merge behind*; (iv) *over-cautious* merge with enlarged headways. This shows the multiplicity of homotopy classes that often (if not always) exist in complex multi-robot systems, that are often impossible to capture with local NE solvers. Local methods can be sensitive to initialization and may remain within a single homotopy class; our search, by construction, explores all classes.

Opposing-lane overtake. We consider a two-lane bidirectional road with oncoming traffic and three robots to simulate risk-aware passing with heterogeneous

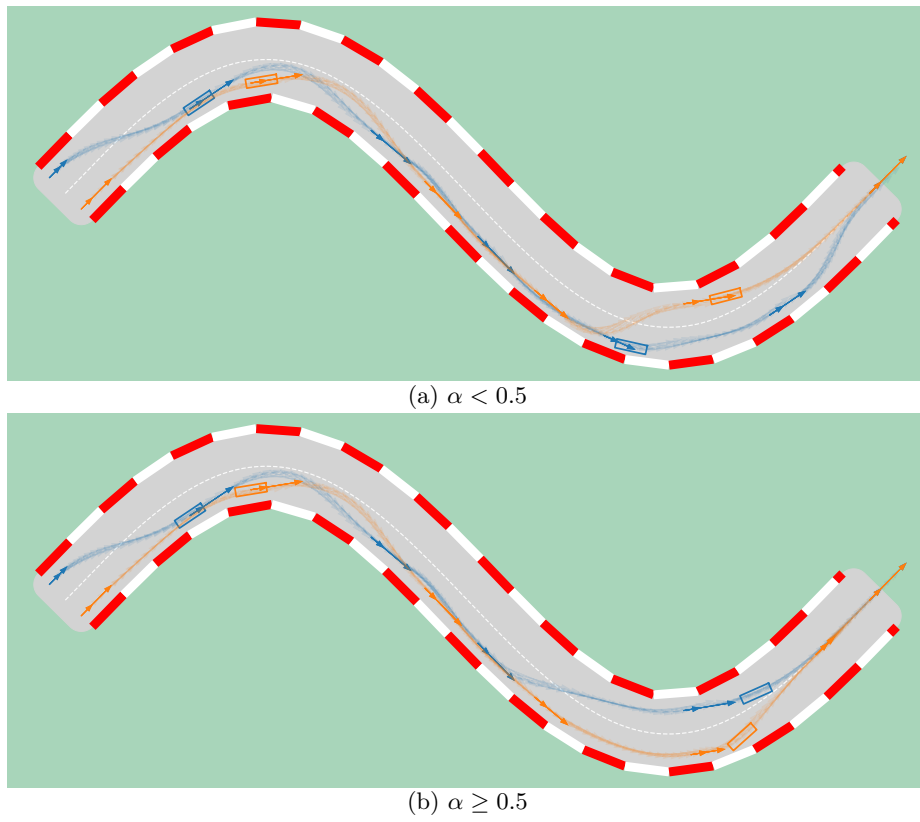


Fig. 4: Racetrack overtake. Prioritized robot takes inside lane at final turn and wins the race. Robot 1 (blue) always blocked at first turn by Robot 2 (orange) despite priority.

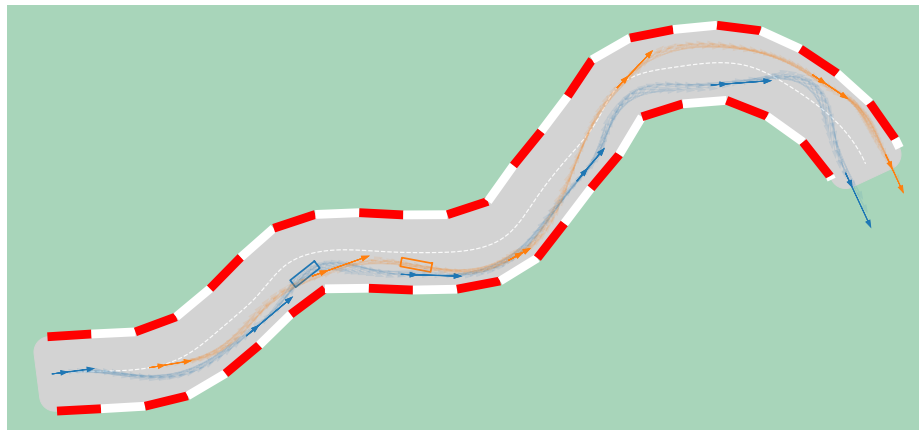
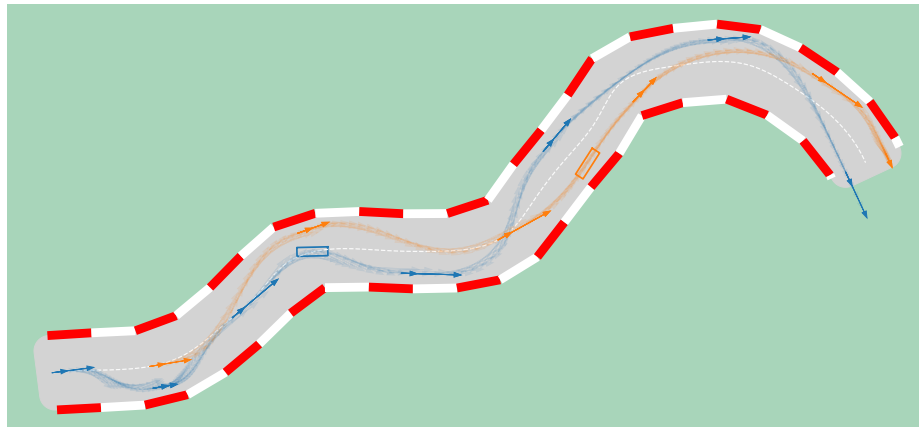
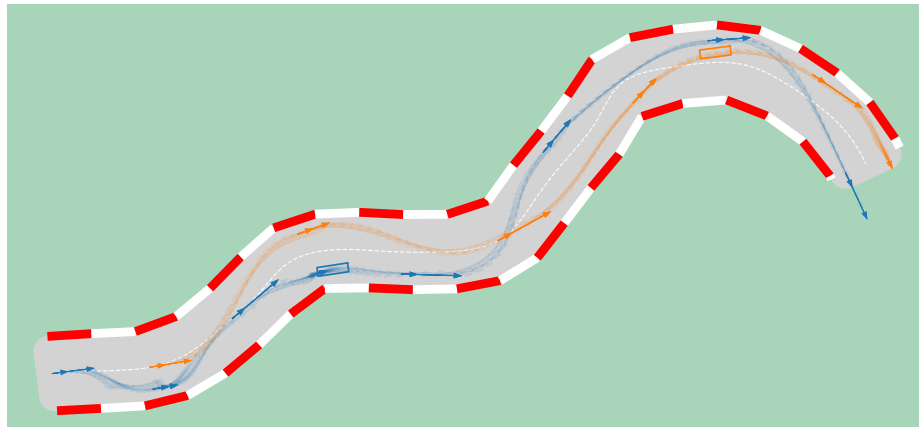
(a) $\lambda_{\text{prox}} = 0.00$ (b) $\lambda_{\text{prox}} = 0.25$ (c) $\lambda_{\text{prox}} \geq 0.50$

Fig. 5: Following distance. Robot 1 (blue) trails at various distances behind Robot 2 (orange) as proximity is more heavily penalized.

capabilities (G^1 has $v \in [0, 10]$, $k = 5$, G^2, G^3 have $v \in [0, 4]$, $k = 3$). We also test how α and λ_{prox} modulate dangerous overtake decisions and select among oncoming-lane vs. in-lane homotopy classes. We set $J = (1 - \alpha)J^1 + \alpha(J^2 + J^3)$, $\alpha \in [0, 1]$, and $\lambda_{\text{prox}} \in [0, 1]$.

In Fig. 6 we see that with high priority and low λ_{prox} , Robot 1 overtakes at the first viable opportunity. Increasing λ_{prox} and lowering priority, however, delays the pass until oncoming traffic clears, and beyond a certain threshold, the NE forgoes the overtake entirely. This too shows extreme behavioural changes across the different homotopy classes, as well as providing (as above) an upper/lower bound on potentially reachable behaviors/outcomes within the NE space.

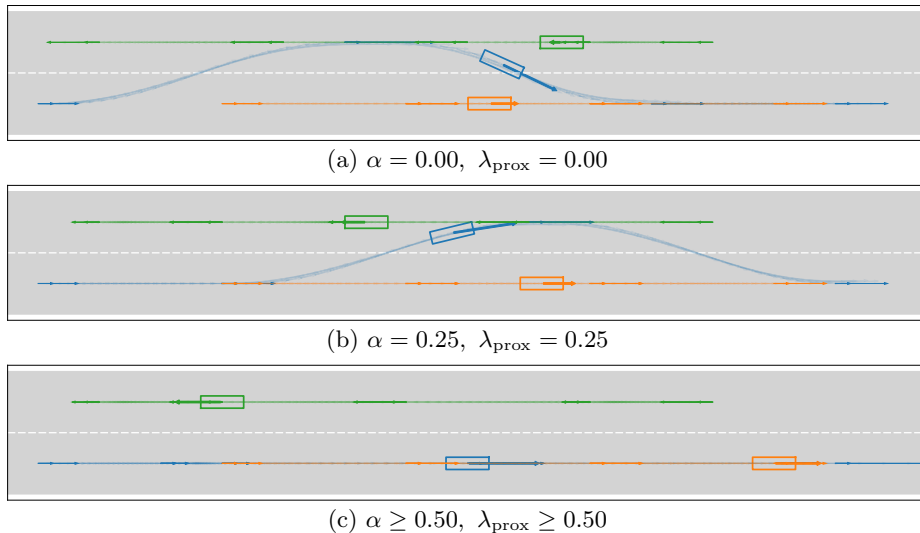


Fig. 6: Ongoing-lane overtake. Robot 1 (blue) tries to overtake Robot 2 (orange) via Robot 3’s (green) opposing lane. Different NE overtake strategies chosen as priority and proximity penalty modulated

6.3 Running time evaluation

Table 1 reports wall-clock solve times for GTNS across several maps, goal distances and number of robots. Dimensions are $|x| \times |y| \times |\theta| \times |v| \times |\delta|$, where $|\cdot|$ is the number of discrete values used for each state variable.

The *Generic Free* map is an obstacle-free workspace used to stress test expansion (maximal branching), whereas *Generic Obstacles* uses the same spatial dimensions but with randomly placed obstacles that prune many nodes/edges (lower branching).

Goal distance D is a conservative proxy for planning horizon T as a time cap T restricts search to the subgraph reachable within $\lfloor T/\Delta t \rfloor$ edges from the

Table 1: Selected graphs with sizes and per-distance solve times. Each row corresponds to a map, number of robots (m). The rightmost block lists time(s) in seconds *with the associated goal distance D in parentheses*, ordered by increasing D .

Map	$ \mathbf{V} $	$ \mathbf{E} $	m	Solve Times (sec) by Distance D						
Generic Free	7,560	51,733	2	3.31(7)	0.046(9)	2.11(11)	1.57(13)	0.063(15)	4.73(17)	
			3	396.1(7)	3.7(9)	59.1(11)	16.2(13)	9(15)	178.5(17)	
Generic Obstacles	6,300	25,818	2	0.051(7)	0.039(9)	1.28(11)	0.666(13)	0.797(15)	0.136(17)	
			3	15.1(7)	34(9)	3.79(11)	12.2(13)	4.58(15)	12(17)	
Two-Lane Road	5,138	39,618	2	0.034(7)	1.02(9)	0.984(11)	0.501(13)	4.59(15)	2.77(17)	
			3	10.7(7)						
Track	693	4,359	2	0.097(7)	0.24(9)	0.435(11)	0.865(13)	0.247(15)	1.55(17)	
			3	60.3(7)	2.22(9)	32.1(11)	55.2(13)	525.9(15)		
Crossroads	1,428	550	2	0.005(2)	0.006(4)	0.004(6)	0.007(7)	0.007(8)		
			3	0.046(2)	0.05(4)	0.045(6)	0.037(7)	0.041(8)		
			4	0.162(2)	0.111(4)	0.154(6)	1.53(7)	0.283(8)		
			5	0.724(2)	1(4)	12.2(6)	4.93(7)	12.1(8)		
			6	0.363(8)						
			7	2.32(8)						

start; by instead varying the goal distance D , we probe increasingly far targets without imposing this cap.

We note that increasing D does not substantially increase running time—a considerable strength of our approach: unlike optimization-based approaches—where running time typically scales with horizon due to the growing number of decision variables—our graph-based formulation keeps per-step local problems fixed-size and searches over a discrete action set, so increasing D does not balloon the optimizer.

By contrast, running time generally increases with the number of robots. The joint neighbor set grows combinatorially, interaction geometry becomes richer (more constraints and blocking situations), and the equilibrium check ISNASHE-EQUILIBRIUM triggers more single-robot A* calls (a principal computational bottleneck) as m grows. An exception is the *Crossroads* map: its branching factor is small and interactions are simple, so adding robots does not markedly increase search effort.

Across all settings, *instance difficulty* (map layout and interaction geometry) dominates running time. Tight merges, opposing-lane passes, and narrow corridors can make some two-robot cases slower—or even infeasible at a given discrete horizon—than multi-robot cases on simpler maps with few viable options. This can also explain why *Generic Obstacles* is faster on average than *Generic Free*: moderate obstacle density reduces branching without making the graph too sparse.

6.4 Comparison with previous short-horizon methods

In this section, we provide a comparison with previous work that can be most directly simulated in our graph-based framework. Specifically, we consider approaches that compute NE through an explicit enumeration of all possible solutions within a bimatrix formulation [24, 39]. As reported in [24], solving just $N = 3$ prediction steps—which corresponds to an horizon of three steps in our setting—requires constructing and brute-force solving two payoff matrices with sizes on the order of 10^{12} —an intractable task. To assess this limitation, we compare the solution cost obtained by GTNS using a long horizon of 17 steps, with that obtained by GTNS attempting the same problem, but only invoked to solve subproblems with horizon 2 in MPC fashion.

As expected, across multiple track scenarios (e.g. those in Fig. 4 and 5), both the individual costs J^i and the team cost J *degraded* relative to the long horizon. The behavior reflects myopia: short horizons optimize locally and replan, while the long horizon equilibrium, enabled by GTNS, anticipates future interactions and coordinates earlier. Although absolute numbers depend on discretization, the trend was consistent: long-horizon joint NE planning dominated short-horizon patching in both cost and qualitative safety. Costs in the short-horizon setting were often 2x the costs of their long-horizon counterparts.

6.5 Effect of NE mismatch

Our approach allows for computing various NE solutions to the same problem. The experimental results indicate that different equilibria can result in vastly distinct performance of the multi-robot system. So far, we have assumed that all the agents execute the same equilibrium, which may not be guaranteed in practice. To motivate further study in coordinating the equilibrium between agents, we evaluate the consequences of equilibrium mismatch.

In the majority of tested cases, when agents executed in an open-loop fashion trajectories belonging to different NEs, collisions between robots were encountered. This underscores the need for a coordinated, team-wide equilibrium in behavior-aware motion planning. To address the concern that open-loop per-agent NEs are “obviously brittle,” we also evaluated an MPC variant: at every step each agent re-solved *its own* NE instance, where $J = J_i$, i.e., the global cost strictly optimizes the solution of the specific robot executing its trajectory from this NE. At every step, the robot resolved the problem towards the goal using this objective while observing the updated locations of the other robots, executed its step, and repeated the process. Such an approach is hoped to be more resilient as it could provide more opportunities for the robots to avoid colliding with each other. Unfortunately, even under this closed-loop regime, the lack of shared equilibrium selection caused systematic issues and in almost all scenarios (e.g. those in Fig. 6 and 3) a collision. In rare “best-case” scenarios, when interaction geometry was simple, (e.g. on the track in Fig. 5 with large start distance) mismatched individual NEs yielded similar solutions to those returned by the global planner.

We believe that such a NE mismatch could explain the cause of motor accidents between human drivers where a driver “fails to judge other driver’s path or speed”, which contributes to at least %13 of all accidents in the US, according to a 2013 report [25], and %11 of fatal accidents in the UK, based on a 2022 report [6]. This suggests that algorithms such as GTNS could be used by transportation engineers to assess the impact, in terms of safety, of introducing a new road feature (e.g., an intersection or a traffic island).

7 Conclusion and future work

We presented Game-Theoretic Nested Search (GTNS), a scalable framework for computing global Nash equilibria for game-theoretic motion planning with general dynamics. GTNS enjoys strong theoretical guarantees, while also allowing explicit selection among multiple equilibria via a user-specified global objective. Across driving and racing scenarios, GTNS finds collision-free, dynamically feasible interactions within seconds.

In the future, we plan to address a key limitation of the approach, which is the reliance on high-fidelity kinodynamic roadmaps, whose construction requires many calls to a BVP solver; although performed offline, and can be reused in different scenarios, the compute cost and memory footprint grow with state discretization and connection density, and are a key practical bottleneck. One possible direction could be substituting such graphs with kinodynamic trees that are computed on-the-fly by sampling-based planners [10, 14, 23]. This modification should be done with care as to ensure that the game-theoretic guarantees hold. We also plan to explore improving the algorithm’s scalability with respect to the number of robots. Although the tensor graph is explored implicitly, joint branching still grows with the number of robots; moreover, each equilibrium check triggers single-robot searches that can dominate running time in tightly coupled scenes. We believe that improved heuristics and pruning conditions, as well as reusing information between subsequent calls of the NE check, and integration with learning-based exploration [13], could significantly speed up the algorithm, as well as parallelizing the single-robot searches.

In the longer run, we plan to develop extensions of the approach to the closed-loop setting, and study principled tie-breaking and fairness-/risk-aware objectives, as well as coordination mechanisms when several NEs exist.

References

1. Andersson, J.A.E., Gillis, J., Horn, G., Rawlings, J.B., Diehl, M.: CasADi – A software framework for nonlinear optimization and optimal control. *Mathematical Programming Computation* **11**(1), 1–36 (2019). <https://doi.org/10.1007/s12532-018-0139-4>
2. Aumann, R.J.: Subjectivity and correlation in randomized strategies. *Journal of mathematical Economics* **1**(1), 67–96 (1974)

3. Burger, C., Fischer, J., Bieder, F., Taş, O.S., Stiller, C.: Interaction-aware game-theoretic motion planning for automated vehicles using bi-level optimization. In: International Conference on Intelligent Transportation Systems. pp. 3978–3985 (2022)
4. Dayan, D., Solovey, K., Pavone, M., Halperin, D.: Near-optimal multi-robot motion planning with finite sampling. *IEEE Transactions on Robotics* (2023)
5. Dellin, C., Srinivasa, S.: A unifying formalism for shortest path problems with expensive edge evaluations via lazy best-first search over paths with edge selectors. In: International Conference on Automated Planning and Scheduling. vol. 26, pp. 459–467 (2016)
6. Department for Transport: Road safety factors: initial analysis. Official statistics, UK Department for Transport, London, UK (May 2024), <https://www.gov.uk/government/statistics/road-safety-factors-initial-analysis/road-safety-factors-initial-analysis>, published 30 May 2024
7. Dezső, B., Jüttner, A., Kovács, P.: LEMON—an open source c++ graph template library. *Electronic Notes in Theoretical Computer Science* **264**(5), 23–45 (2011)
8. Fisac, J.F., Bronstein, E., Stefansson, E., Sadigh, D., Sastry, S.S., Dragan, A.D.: Hierarchical game-theoretic planning for autonomous vehicles. In: International conference on robotics and automation. pp. 9590–9596. IEEE (2019)
9. Fridovich-Keil, D., Ratner, E., Peters, L., Dragan, A.D., Tomlin, C.J.: Efficient iterative linear-quadratic approximations for nonlinear multi-player general-sum differential games. In: IEEE international conference on robotics and automation. pp. 1475–1481. IEEE (2020)
10. Fu, M., Solovey, K., Salzman, O., Alterovitz, R.: Toward certifiable optimal motion planning for medical steerable needles. *Int. J. Robotics Res.* **42**(10), 798–826 (2023)
11. Gao, Y., Piccinini, M., Zhang, Y., Wang, D., Moller, K., Brusnicki, R., Zarrouki, B., Gambi, A., Totz, J.F., Storms, K., et al.: Foundation models in autonomous driving: A survey on scenario generation and scenario analysis. arXiv preprint arXiv:2506.11526 (2025)
12. Hart, P.E., Nilsson, N.J., Raphael, B.: A formal basis for the heuristic determination of minimum cost paths. *IEEE Transactions on Systems Science and Cybernetics* **4**(2), 100–107 (1968)
13. Hassidof, Y., Jurgenson, T., Solovey, K.: Train-once plan-anywhere kinodynamic motion planning via diffusion trees. In: Conference on Robot Learning. pp. 1847–1878. PMLR (2025)
14. Hauser, K., Zhou, Y.: Asymptotically optimal planning by feasible kinodynamic planning in a state-cost space. *IEEE Trans. Robotics* **32**(6), 1431–1443 (2016)
15. Hönig, W., de Haro, J.O., Toussaint, M.: db-A*: Discontinuity-bounded search for kinodynamic mobile robot motion planning. In: IEEE/RSJ International Conference on Intelligent Robots and Systems. pp. 13540–13547. IEEE (2022)
16. Jiang, C., Cornman, A., Park, C., Sapp, B., Zhou, Y., Anguelov, D., et al.: Motion-diffuser: Controllable multi-agent motion prediction using diffusion. In: IEEE/CVF conference on computer vision and pattern recognition. pp. 9644–9653 (2023)
17. Kavraki, L.E., Svestka, P., Latombe, J.C., Overmars, M.H.: Probabilistic roadmaps for path planning in high-dimensional configuration spaces. *IEEE transactions on Robotics and Automation* **12**(4), 566–580 (1996)
18. Kleinbort, M., Granados, E., Solovey, K., Bonalli, R., Bekris, K.E., Halperin, D.: Refined analysis of asymptotically-optimal kinodynamic planning in the state-cost space. In: IEEE International Conference on Robotics and Automation. pp. 6344–6350 (2020)

19. LaValle, S.M.: Planning algorithms. Cambridge university press (2006)
20. Le Cleac’h, S., Schwager, M., Manchester, Z.: Lucidgames: Online unscented inverse dynamic games for adaptive trajectory prediction and planning. *IEEE Robotics and Automation Letters* **6**(3), 5485–5492 (2021)
21. Le Cleac’h, S., Schwager, M., Manchester, Z.: Algames: a fast augmented lagrangian solver for constrained dynamic games. *Autonomous Robots* **46**(1), 201–215 (2022)
22. Lee, N., Choi, W., Vernaza, P., Choy, C.B., Torr, P.H., Chandraker, M.: Desire: Distant future prediction in dynamic scenes with interacting agents. In: *IEEE conference on computer vision and pattern recognition*. pp. 336–345 (2017)
23. Li, Y., Littlefield, Z., Bekris, K.E.: Asymptotically optimal sampling-based kinodynamic planning. *The International Journal of Robotics Research* **35**(5), 528–564 (2016)
24. Liniger, A., Lygeros, J.: A noncooperative game approach to autonomous racing. *IEEE Transactions on Control Systems Technology* **28**(3), 884–897 (2019)
25. Najm, W.G., Ranganathan, R., Srinivasan, G., Smith, J.D., Toma, S., Swanson, E., Burgett, A.: Description of light-vehicle pre-crash scenarios for safety applications based on vehicle-to-vehicle communications. Technical Report DOT HS 811 731, U.S. Department of Transportation, National Highway Traffic Safety Administration, Washington, DC (2013), <https://www.nhtsa.gov/sites/nhtsa.gov/files/811731.pdf>
26. Nash Jr, J.F.: Equilibrium points in n-person games. *Proceedings of the national academy of sciences* **36**(1), 48–49 (1950)
27. Nisan, N., Roughgarden, T., Tardos, E., Vazirani, V.V. (eds.): *Algorithmic Game Theory*. Cambridge University Press, Cambridge, UK (2007)
28. Rowold, M., Langmann, A., Lohmann, B., Betz, J.: Open-loop and feedback nash trajectories for competitive racing with iLQGames. In: *IEEE International Conference on Intelligent Transportation Systems*. pp. 1827–1834 (2024)
29. Rudenko, A., Palmieri, L., Herman, M., Kitani, K.M., Gavrila, D.M., Arras, K.O.: Human motion trajectory prediction: A survey. *The International Journal of Robotics Research* **39**(8), 895–935 (2020)
30. Salzmann, T., Ivanovic, B., Chakravarty, P., Pavone, M.: Trajectron++: Dynamically-feasible trajectory forecasting with heterogeneous data. In: *European Conference on Computer Vision*. pp. 683–700. Springer (2020)
31. Schmerling, E., Janson, L., Pavone, M.: Optimal sampling-based motion planning under differential constraints: the drift case with linear affine dynamics. In: *IEEE Conference on Decision and Control*. pp. 2574–2581 (2015)
32. Schmerling, E., Janson, L., Pavone, M.: Optimal sampling-based motion planning under differential constraints: The driftless case. In: *IEEE International Conference on Robotics and Automation*. pp. 2368–2375 (2015)
33. Schmerling, E., Leung, K., Vollprecht, W., Pavone, M.: Multimodal probabilistic model-based planning for human-robot interaction. In: *IEEE International Conference on Robotics and Automation*. pp. 3399–3406. IEEE (2018)
34. Shoham, Y., Leyton-Brown, K.: *Multiagent Systems: Algorithmic, Game-Theoretic, and Logical Foundations*. Cambridge University Press, Cambridge, UK (2009)
35. Shome, R., Kavraki, L.E.: Asymptotically optimal kinodynamic planning using bundles of edges. In: *IEEE International Conference on Robotics and Automation*. pp. 9988–9994 (2021)

36. Shome, R., Solovey, K., Dobson, A., Halperin, D., Bekris, K.E.: dRRT^{*}: Scalable and informed asymptotically-optimal multi-robot motion planning. *Auton. Robots* **44**(3-4), 443–467 (2020)
37. Solovey, K., Salzman, O., Halperin, D.: Finding a needle in an exponential haystack: Discrete RRT for exploration of implicit roadmaps in multi-robot motion planning. *The International Journal of Robotics Research* **35**(5), 501–513 (2016)
38. Spica, R., Cristofalo, E., Wang, Z., Montijano, E., Schwager, M.: A real-time game theoretic planner for autonomous two-player drone racing. *IEEE Transactions on Robotics* **36**(5), 1389–1403 (2020)
39. Tikna, A., Roveri, M., Fontanelli, D., Palopoli, L.: When graphs meet game theory: a scalable approach for robotic car racing. In: *IEEE Computers, Software, and Applications Conference*. pp. 1–8. IEEE (2023)
40. Tsaknakis, H., Spirakis, P.G.: An optimization approach for approximate nash equilibria. *Internet Math.* **5**(4), 365–382 (2008)
41. Wang, M., Wang, Z., Talbot, J., Gerdes, J.C., Schwager, M.: Game-theoretic planning for self-driving cars in multivehicle competitive scenarios. *IEEE Transactions on Robotics* **37**(4), 1313–1325 (2021)
42. Wang, Y., Xing, S., Can, C., Li, R., Hua, H., Tian, K., Mo, Z., Gao, X., Wu, K., Zhou, S., You, H., Peng, J., Zhang, J., Wang, Z., Song, R., Yan, M., Zimmer, W., Zhou, X., Li, P., Lu, Z., Chen, C.J., Huang, Y., Rossi, R.A., Sun, L., Yu, H., Fan, Z., Yang, F.H., Kang, Y., Greer, R., Liu, C., Lee, E.H., Di, X., Ye, X., Ren, L., Knoll, A., Li, X., Ji, S., Tomizuka, M., Pavone, M., Yang, T., Du, J., Yang, M.H., Wei, H., Wang, Z., Zhou, Y., Li, J., Tu, Z.: Generative ai for autonomous driving: Frontiers and opportunities (2025)
43. Wu, C., Kreidieh, A.R., Parvate, K., Vinitsky, E., Bayen, A.M.: Flow: A modular learning framework for mixed autonomy traffic. *IEEE Transactions on Robotics* (2021)
44. Wurman, P.R., Barrett, S., Kawamoto, K., MacGlashan, J., Subramanian, K., Walsh, T.J., Capobianco, R., Devlic, A., Eckert, F., Fuchs, F., et al.: Outracing champion gran turismo drivers with deep reinforcement learning. *Nature* **602**(7896), 223–228 (2022)
45. Zhu, E.L., Borrelli, F.: A sequential quadratic programming approach to the solution of open-loop generalized nash equilibria. In: *IEEE International Conference on Robotics and Automation*. pp. 3211–3217. IEEE (2023)

A Additional Figures

Table 2: Notation for continuous and graph-based multi-robot planning.

SR Symbol	MR Symbol	Meaning
$[m]$		Robot index set $\{1, \dots, m\}$
d_i, D_i		Dim. of $\mathcal{X}^i \subseteq \mathbb{R}^{d_i}, \mathcal{U}^i \subseteq \mathbb{R}^{D_i}$
\mathcal{X}^i	$\mathcal{X} = \times_{i=1}^m \mathcal{X}^i$	Robot i (joint) state space
\mathcal{U}^i	$\mathcal{U} = \times_{i=1}^m \mathcal{U}^i$	Robot i (joint) control space
$\mathcal{X}_f^i \subset \mathcal{X}^i$	$\mathcal{X}_f = \times_{i=1}^m \mathcal{X}_f^i \subset \mathcal{X}$	Collision-free state space
\mathcal{U}_T^i	$\mathcal{U}_T = \times_{i=1}^m \mathcal{U}_T^i$	Admissible controls $u^i : [0, T] \mapsto \mathcal{U}^i$ ($u : [0, T] \mapsto \mathcal{U}$)
$x^i(t)$	$x(t) = (x^1(t), \dots, x^m(t))$	Robot i (joint) state at time $t \in [0, T]$
$u^i(t)$	$u(t) = (u^1(t), \dots, u^m(t))$	Robot i (joint) control at time $t \in [0, T]$
x_0^i	x_0	Robot i (joint) initial state
$\mathcal{X}_{\text{goal}}^i$	$\mathcal{X}_{\text{goal}} = \times_{i=1}^m \mathcal{X}_{\text{goal}}^i$	Robot i (joint) goal region
$\pi_{x_0, u}^i$	$\pi_{x_0, u} = \times_{i=1}^m \pi_{x_0, u}^i$	Robot i (joint) continuous trajectory $[0, T] \mapsto \mathcal{X}^i$ ($[0, T] \rightarrow \mathcal{X}$)
Π^i	$\Pi = \times_{i=1}^m \Pi_n^i$	All robot i (joint) feasible continuous trajectories
$c^i(\pi^i(t), \pi^{-i}(t))$		Stage cost of robot i given others' trajectories
	$c(\pi(t))$	Stage cost over joint trajectory
$J^i(\pi^i, \pi^{-i})$		Cost of robot i given others' trajectories
	$J(\pi)$	Global cost over joint trajectory in time window $[0, T]$
$f^i(x^i, u^i)$	$f(x, u)$	Robot i (joint) dynamics: $\dot{x}^i(t) = f^i(x^i(t), u^i(t))$ ($\dot{x}(t) = f(x(t), u(t))$)
Δt		Fixed duration of each edge
$G^i = (V^i, E^i)$	$G = (V, E)$	Robot i (joint, tensor-product) graph
V^i	$V = \times_{i=1}^m V^i$	Robot i (joint) sampled states $x^i \in \mathcal{X}^i$ incl. $x_0^i, \mathcal{X}_{\text{goal}}^i$ ($x \in \mathcal{X}$ incl. $x_0, \mathcal{X}_{\text{goal}}$)
E^i	$E = \times_{i=1}^m E^i$	Robot i (joint) edges $e^i = (x^i, y^i)$ ($e = (x, y)$) with control $u_{e^i}^i \in \mathcal{U}_{\Delta t}^i$ ($u_e \in \mathcal{U}_{\Delta t}$)
$\pi_{e^i}^i$	$\pi_e = (\pi_{e_1}^1, \dots, \pi_{e^m}^m)$	Robot i (joint) trajectory along edge e^i (e)
$\pi_n^i = (x_{e_1^i}^i, \dots, x_{e_n^i}^i)$	$\pi_n = (x_{e_1}, \dots, x_{e_n})$	Robot i (joint) n -step trajectory on G^i (G)
Π_n^i	$\Pi_n = \times_{i=1}^m \Pi_n^i$	Robot i (joint) feasible n -step trajectories
	ε	Approximation factor for ε -equilibrium

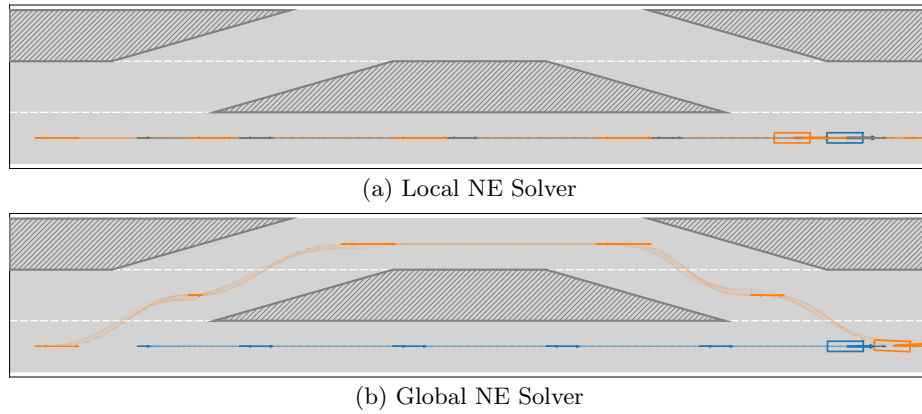


Fig. 7: Local vs. global Nash equilibrium (NE) in a narrow-overtake scenario, where Robot 1 (blue) is attempting to overtake Robot 2 (orange). (a) A local, initialization-dependent solver converges to a non-overtake NE within the homotopy class implied by its seed. (b) Our global NE method searches across homotopy classes and discovers here the overtaking NE.

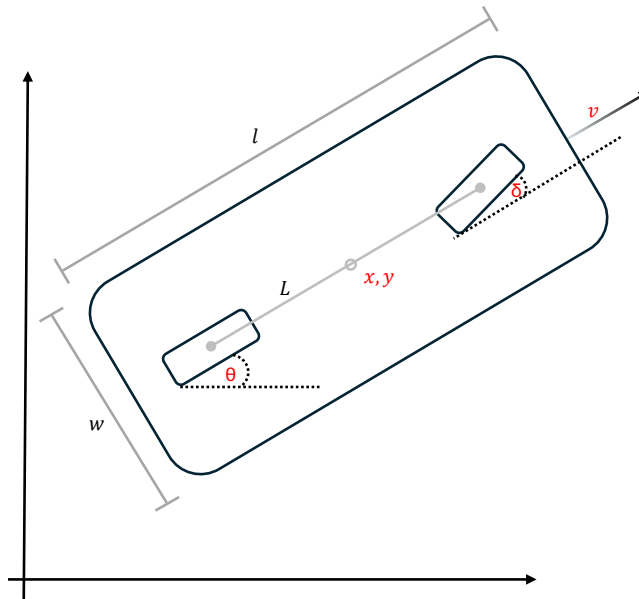


Fig. 8: Second-order bicycle model for car dynamics. Car dimensions l, w, L in black; State variables $(x, y, \theta, v, \delta)$ in red.

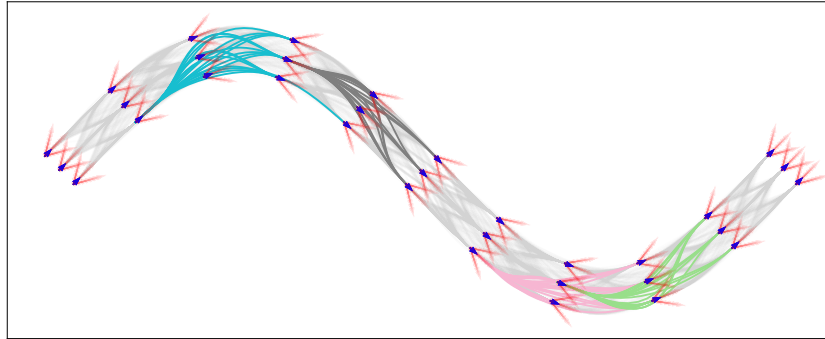


Fig. 9: Kinodynamic *track graph* built from racetrack centerline with lateral offsets. Node, edge styling as in grid-graph.